J Solid State Electrochem (2012) 16:3059–3067
DOI 10.1007/s10008-012-1746-z

ORIGINAL PAPER

Effect of cyclic oxidation on electrochemical corrosion of type 409 stainless steel in the simulated muffler condensates

Mou Cheng Li · Shi Dong Wang · Rong Yao Ma · Pei Hong Han · Hong Yun Bi

Received: 28 December 2011 / Revised: 17 March 2012 / Accepted: 8 April 2012 / Published online: 25 April 2012

Abstract The electrochemical corrosion behavior of 409 stainless steel after cyclic oxidation below 400 °C was investigated in the simulated muffler condensates by using surface analysis and electrochemical measurement techniques. In the cyclic processes of condensate-dipping and oxidation, specimens may form defective oxide films and weak Cr depletion underlying the oxide films. Sulfate from the condensate-dipping will give rise to sulfidation during the cyclic oxidation, being detrimental to both the oxidation and corrosion properties of stainless steel. The oxidation above 300 °C deteriorates the corrosion resistance, even leading to active corrosion in the acidic condensate solutions. Comparatively, specimens oxidized cyclically without condensate-dipping show much higher condensate corrosion resistance. It is suggested that the acidic condensate corrosion is accelerated by the synergetic effect of oxidation and condensation in the mufflers, and then may result in perforation through the defects such as cracks and nodules in oxide films on the stainless steel surface.

Keywords Stainless steel · Corrosion · Oxidation · Automotive exhaust system · Condensation

M. C. Li (✉) · S. D. Wang · R. Y. Ma · P. H. Han
Institute of Materials, Shanghai University,
149 Yanchang Road,
Shanghai 200072, China
e-mail: mouchengli@shu.edu.cn

H. Y. Bi
Stainless Steel Technical Centre, Baoshan Iron and Steel Co., Ltd.,
580 Changjiang Road,
Shanghai 200431, China

Introduction

Automotive exhaust system serves to reduce noise and waste gas emissions produced by the engine. It usually can be divided into two parts, i.e., the hot end and the cold end. Nowadays, both hot and cold end components are manufactured extensively from stainless steels, especially ferritic stainless steels due to the lower cost in comparison with austenitic steels [1–3]. The cold end components mainly include muffler and tail pipe. In the case of short driving trips or frequent run-stop changes, the temperature of exhaust gas often drops below its dewpoint in the cold end [3]. This inevitably induces gas condensation and ensuing aqueous corrosion inside the components, particularly the muffler with complicated internal structures. On the other hand, during long driving journeys, the high temperature exhaust gas may heat the cold end components up to about 400 °C, leading to condensation evaporation and slight thermal oxidation [1–9]. Thus, the oxidation and corrosion problems of the cold end components deserve special attentions with the rapid development of automotive industry.

Condensate corrosion is the major internal corrosion in the muffler and other cold end components. The condensed water contains normally SO_4^{2-}, CO_3^{2-}, Cl^-, NO_3^-, NH^+, organic acids, and so on, mainly resulted from the combustion of fuel oil [2–8]. Another source of Cl^- ions is the chloride compounds remained in the catalytic converters from the deposition process of precious metal catalysts [3]. Corrosion perforation of mufflers takes place frequently and has great influence on the lifetime (or warranty) of automobiles. This is related conventionally to pitting corrosion due to the existence of Cl^- ions in condensate solutions [10]. The initial pH value of condensed water is about 8 to 9. With the run-stop repeat of automobile, the condensates tend to become more aggressive because of the accumulation of these ions and decrease of pH

value to about 3 through water evaporation [3, 10]. Though SO_4^{2-}, Cl^-, and low pH are broadly believed as main factors affected condensate corrosion, their effect will change markedly with the sulfur content of fuel, driving process, and atmospheric pollutants.

Thermal oxidation (≤400 °C) exerts great influence on the condensate corrosion in exhaust systems. In order to evaluate the materials for cold end components, thermal oxidation is adopted as a pretreatment or a cyclic step in the accelerated tests such as dip-dry test [6] and cyclic condensation test [2, 4]. Kim et al. [11] found that condensate corrosion of stainless steels was inhibited by pre-oxidation below 380 °C but was enhanced by pre-oxidation above 380 °C, which depended on the compactness of thin oxide layers formed on the steel surfaces. Typical cyclic tests of condensate corrosion set a heating step at 130 °C (Nippon Steel) [2] or 250 °C (AK Steel, Allegheny Ludlum) [12, 13] to simulate thermal environment inside the mufflers. Obviously, there is very limited mechanism information on the internal corrosion of the cold end components under the cyclic conditions of thermal oxidation and condensation.

As what occurred in the oxidation of stainless steels with salts above 600 °C [14–16], the electrolyte condensed from exhaust gas would play an important role in the thermal oxidation of the cold end components. In this work, cyclic oxidation was performed below 400 °C for type 409 stainless steel (409 SS) with or without condensate-dipping before each oxidation step. Subsequently, electrochemical corrosion of oxidized 409 SS specimens was comparatively investigated in the simulated muffler condensates. The main purpose is to gain an insight into influence of cyclic oxidation on condensate corrosion of stainless steels for automotive exhaust systems.

Experimental

Test material and solution

Specimens with a dimension of 20×10×0.5 mm were fabricated from a commercial type 409 SS plate, a (Ti, Nb)-bearing ferritic steel. The chemical composition is given in Table 1. Prior to each experiment, the specimen was ground with 800 grit waterproof abrasive paper and cleaned with ethanol and distilled water.

According to the literature [3, 12], test solution was prepared as 52.1 mM $(NH_4)_2SO_4$+2.8 mM NH_4Cl+ 1.6 mM NH_4NO_3+2.2 mM HCOOH with analytical grade reagents and distilled water. In order to simulate the acidic gas condensates as mentioned, the pH value was adjusted to 3 with dilute H_2SO_4 solution. This would represent typically an accelerated corrosion environment for automobiles with high sulfur-fuel oil as used in China [17].

Cyclic oxidation and electrochemical measurement

As shown in Table 2, cyclic dip-dry test (DDT) and pure oxidation test (POT) were adopted to comparatively elucidate the temperature and condensation effect on cyclic oxidation of 409 SS in automotive exhaust system. For one cyclic experiment, DDT included four steps successively, while POT only had two steps without dipping in the condensate solution. Each heating step was conducted in a muffle at the given temperature under atmosphere condition with corundum crucibles. Three specimens were used for the tests at each temperature (i.e., 250 °C, 300 °C, or 400 °C). As for DDT, only 1 min of condensate-dipping was carried out in test solution at 80 °C to lead aggressive ions into the subsequent oxidation and simultaneously to avoid the corrosion of 409 SS during the immersion.

Electrochemical corrosion experiments were performed in a three-electrode glass cell containing 200 mL test solution at 80 °C. An air cooling duct was used to prevent water outlet through evaporation. A saturated calomel electrode (SCE) connected to a Luggin capillary was used as the reference electrode and a platinum foil as the counter electrode. The solution in Luggin capillary could reach about 40 °C. After ten cycles of DDT or POT, the oxidized specimens were welded with copper wires and immersed partially (about 2 cm^2) in the test solutions, which served as the working electrodes in the electrochemical measurements.

Corrosion potential was measured from the beginning of experiment for 1 h. Then, electrochemical impedance spectroscopy (EIS) and anodic polarization studies were conducted successively on the electrode. These were performed through a PAR (Princeton Application Research, AMETEK, Inc.) system, which comprised an M273A potentiostat/galvanostat, an M5210 lock-in amplifier and the PowerSuite software. During EIS measurement, an alternating current signal with the frequency range from 20 kHz to 0.01 Hz and amplitude of 10 mV (rms) was applied on the working electrode at the corrosion potential. EIS spectra were interpreted using the ZSimpWin 3.21 software (a nonlinear least square fitting procedure). Anodic polarization curve was measured at a potential scan rate of 20 mV min^{-1} from the

Table 1 Chemical composition of 409 SS specimens

Element	C	P	S	Si	Mn	Cr	Ti	Nb	N	Al	Ni
Mass (wt.%)	0.014	0.025	0.0012	0.51	0.22	11.5	0.16	0.19	0.008	0.01	0.07

Table 2 Procedure of dip-dry test and pure oxidation test

Step	DDT	POT
1	Heating at 250 °C, 300 °C, or 400 °C for 1 h	Heating at 250 °C, 300 °C, or 400 °C for 1 h
2	Cooling at ambient temperature for 20 min	Cooling at ambient temperature for 30 min
3	Immersion in test solution at 80 °C for 1 min	/
4	Drying with hot air	/

corrosion potential to the electrode potential with a current density of 1 mA cm^{-2}.

Surface analysis

The oxidized and corroded specimens were observed using scanning electron microscopy (SEM) (FEI XL30) with energy dispersive analysis of X-rays (EDAX). X-ray diffraction (XRD) studies were carried out by using a Rigaku diffractometer (D/MAX 2550 V) with Cu Kα irradiation (λ= 0.15405 nm). The depth profiles of oxide films formed on 409 SS surfaces were analyzed using glow discharge optical emission spectroscopy (GDOES) (LECO GDS 850A). Profiling was carried out at a pressure of 800 Pa and a power of 40 W in an argon atmosphere with a sampling time of 10 ms from a circular specimen area of about 4 mm in diameter.

Results

Characteristics of oxidized specimen surfaces

Figure 1 shows surface images for specimens after ten cycles of POT at different heating temperature. After oxidation at 250 °C, the specimen remained its original grinding traces completely, indicative of too thin oxide film to be observed on the surface. At 300 °C, tiny oxide particles formed on the surface, particularly on the edges of grinding traces. As for 400 °C, there were nodular oxides on the surface. It was evident that the growth of oxides became faster with the increase of oxidation temperature from 250 °C to 400 °C.

As seen in Fig. 2, for the specimens after ten cycles of DDT at different temperature, the oxides on the surface evolved from scattered plates to thick scales with increasing the oxidation temperature from 250 °C to 400 °C. The grinding traces were faintly visible at 300 °C but disappeared fully at 400 °C. There were some defects such as pores and cracks in the oxide films. EDAX analysis found small amount of sulfur in the oxides, which meant the existence of sulfate or sulfide. Compared simply with POT, DDT produced much more oxides on specimen surfaces at each corresponding temperature.

After ten cycles of DDT and POT at 400 °C, respectively, the specimen surfaces were analyzed by XRD, as shown in Fig. 3. The oxide films on both specimens were mainly composed of $(Fe, Cr)_2O_3$, but the specimen with DDT showed stronger response peaks than with POT. As for DDT, there also have a small amount of Fe_3O_4 and sulfides FeS and CrS [15, 18]. Because CrS has almost the same response peaks as FeS, it was not marked in Fig. 3. Specimens oxidized at 300 °C or 250 °C presented similar XRD peaks but with weaker response (not shown here). From GDOES measurements, the elemental depth profiles of 400 °C-oxidized specimen surfaces were obtained and are shown in Fig. 4. Both oxide films could be described with bi-layer structure, i.e., the outer layer of iron oxides and the inner layer of chromium-rich oxides. There were weak depletion zones of chromium under the oxide films due to its preferential consumption during cyclic oxidation. These features were similar to those of metal/oxide film interfaces formed around 400 °C on austenitic stainless steels [19, 20]. However, the thickness of oxide film for DDT was obviously larger than for POT. It is seen in Fig. 4 that sulfur element existed in the oxide film for DDT and almost reached metal substrate, but only negligible sulfur response was observed

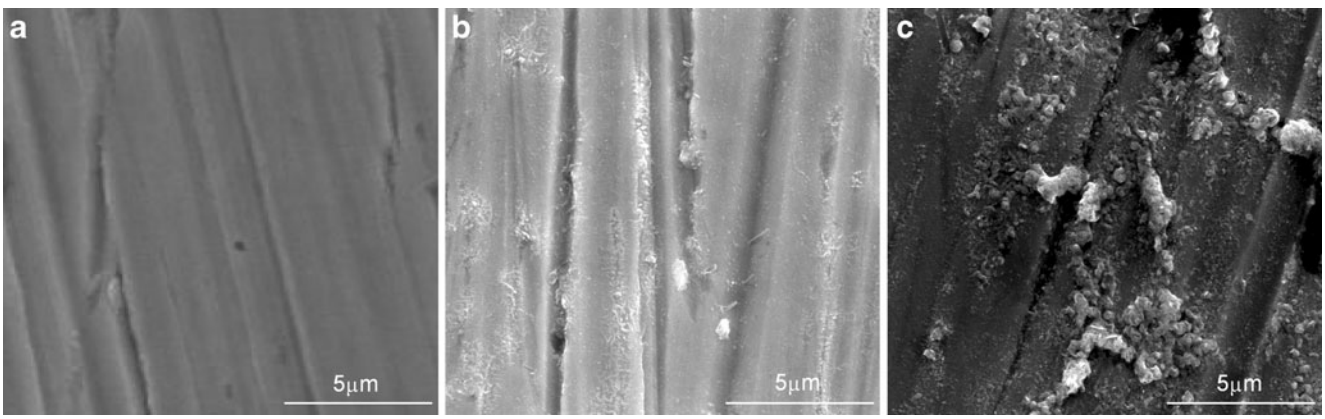

Fig. 1 SEM morphologies of specimen surfaces after ten cycles of oxidation with POT at different temperatures: **a** 250 °C, **b** 300 °C, and **c** 400 °C

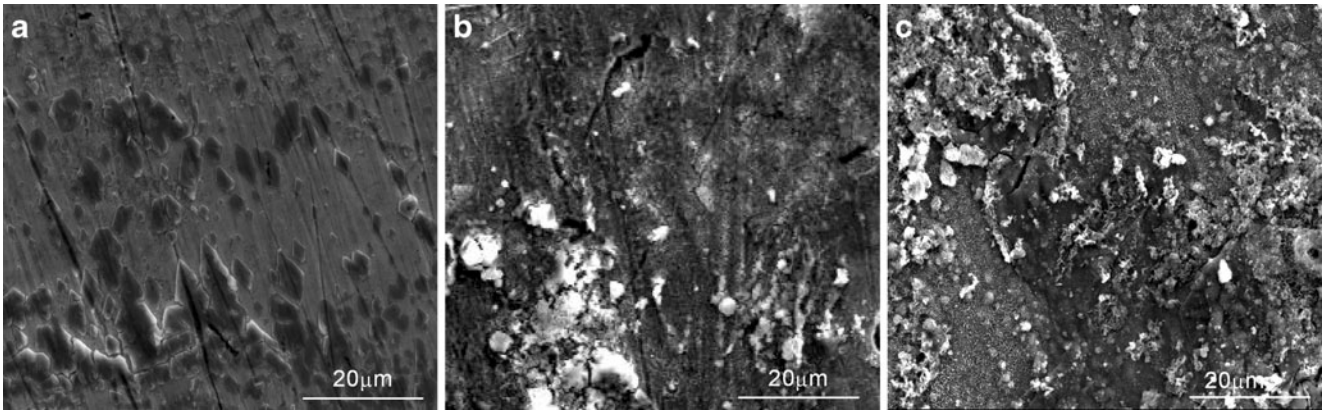

Fig. 2 SEM morphologies of specimen surfaces after ten cycles of oxidation with DDT at different temperatures: **a** 250 °C, **b** 300 °C, and **c** 400 °C

at the oxide film surface for POT. In addition, oxygen response was very strong in the outer layer of each oxide film, which might be far higher than the stoichiometric values in iron oxides (e.g., Fe_2O_3). This could be attributed to the rough and defective nature of oxidized specimen surfaces [21], as observed by SEM in Figs. 1 and 2.

Corrosion potential measurements

Figure 5 shows the time dependence of corrosion potential of the specimens after ten cycles of POT or DDT at different temperature. For the specimens oxidized with POT at 250 °C and 300 °C and with DDT at 250 °C, corrosion potentials changed slightly to reach steady-state values of about 0.44, 0.36 and 0.38 V_{SCE}, respectively. When the specimens were oxidized with POT at 400 °C and with DDT at 300 °C, the corrosion potentials showed sharp drops over 0.4 V before stabilized gradually at about −0.31 and −0.13 V_{SCE}, respectively. As for the specimen oxidized with DDT at 400 °C, the corrosion potential decreased quickly at first and then increased to reach a relatively steady value of about −0.36 V_{SCE}. In order to show the influence of oxidation, the corrosion potential of 409 SS without any oxidation (i.e., unoxidized specimen) is also given here. Apparently, the stable potential values of both 400 °C-oxidized specimens were very close to that of unoxidized specimen (about −0.33 V_{SCE}).

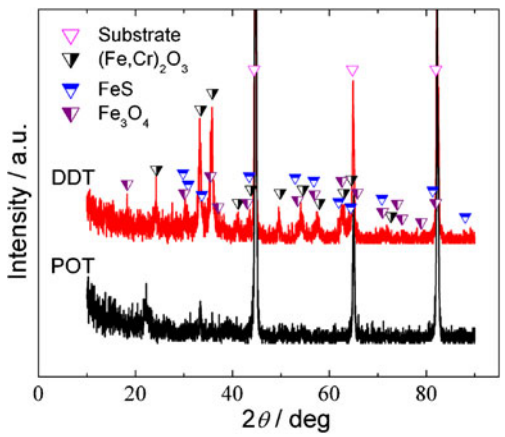

Fig. 3 XRD patterns of specimens oxidized cyclically with POT or DDT at 400 °C

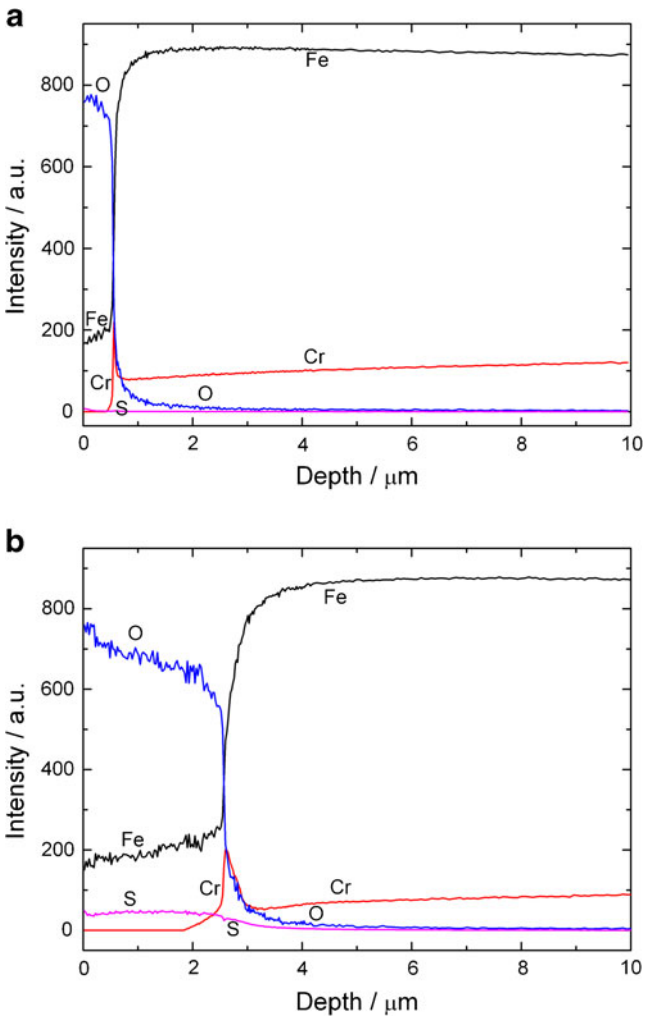

Fig. 4 GDOES depth profiles of specimens oxidized cyclically at 400 °C with **a** POT and **b** DDT

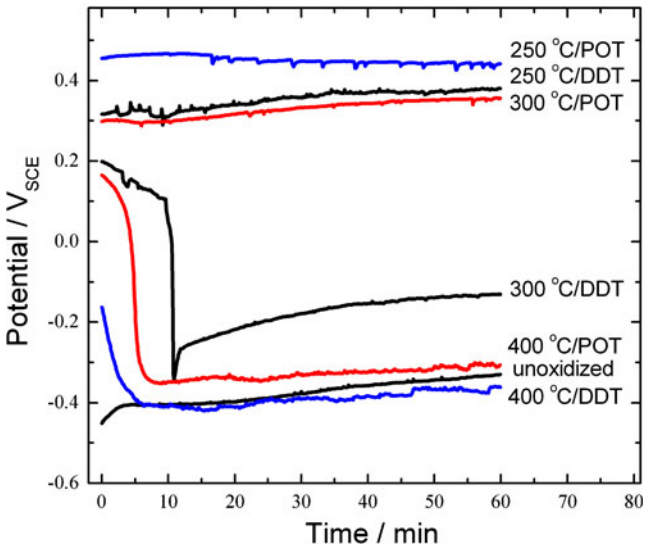

Fig. 5 Time dependence of corrosion potentials for specimens oxidized with POT or DDT at different temperature

EIS spectra

Figures 6 and 7 show the complex-plane impedance and phase angle diagrams measured on the specimens with different oxidation processes. Experimental data were also compared with the fitted values obtained from data processing as described later. There was a similar impedance feature for all specimens, i.e., one capacitive semicircle or two overlapped semicircles over the whole frequency range in Nyquist plots. The semicircles were depressed to a certain extent. Moreover, the semicircle sizes and phase angle peaks in Bode plots tended to decrease significantly with increasing the oxidation temperature from 250 °C to 400 °C for both POT and DDT. As the temperature increased to 400 °C for POT and 300 °C for DDT, the semicircle sizes were changed to lower than that of unoxidized specimen. In addition, the semicircle size for DDT was much lower than that for POT at each given temperature. It is obvious that both condensate-dipping and heating temperature during cyclic oxidation had great influence on the impedance values of oxidized specimens.

Anodic polarization curves

After above EIS measurements on the specimens, anodic polarization curves were measured and are shown in Fig. 8. It is seen that 409 SS without any oxidation was in passive state at the free corrosion potential in the test solution with a passive current density of about 5.5 μA cm^{-2}. After cyclic oxidation with POT at 250 and 300 °C or with DDT at 250 °C, the specimens showed far higher self-passivation ability than the unoxidized specimen. On the contrary, the cyclic oxidation with DDT at 300 °C resulted in a poor passive state with the passive current density larger than 37 μA cm^{-2}. The cyclic oxidation with POT or DDT at 400 °C would give rise to active corrosion. Furthermore, specimens except DDT at 400 °C displayed transpassivation peaks at about 0.84 V_{SCE} [22, 23] and oxygen evolutions starting from about 1.15 V_{SCE}.

Figure 9 gives SEM morphologies of the specimen surfaces after polarization measurements. As for POT, the specimens oxidized at 250 and 300 °C almost remained the grinding surfaces without significant anodic dissolution, but there formed small pits on the surface of 400 °C-oxidized specimen. As for DDT, there were some pits on all three specimen surfaces, especially on the 400 °C-oxidized specimen. It should also be noted that the thermal oxide nodules formed through POT at 400 °C (Fig. 1) and DDT at 300 °C (Fig. 2) could hardly be observed again on the specimens.

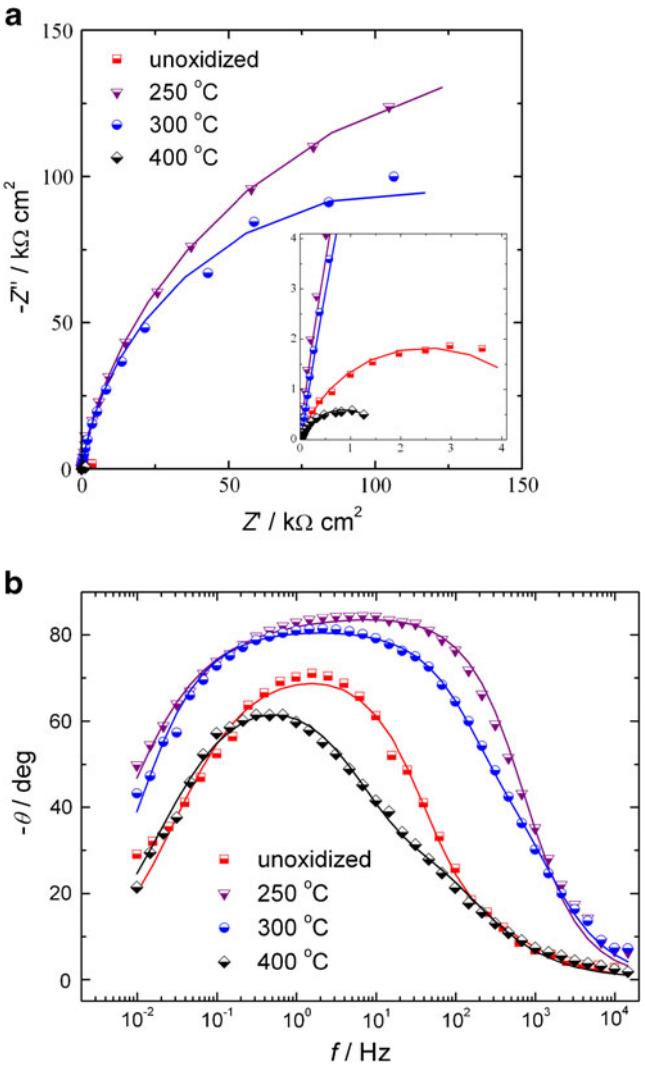

Fig. 6 Impedance plots for specimens without oxidation and with POT in the test solutions: **a** Nyquist plots; **b** Bode plots. *Symbols*: experimental data; *lines*: fitted values; *insets*: the high frequency parts

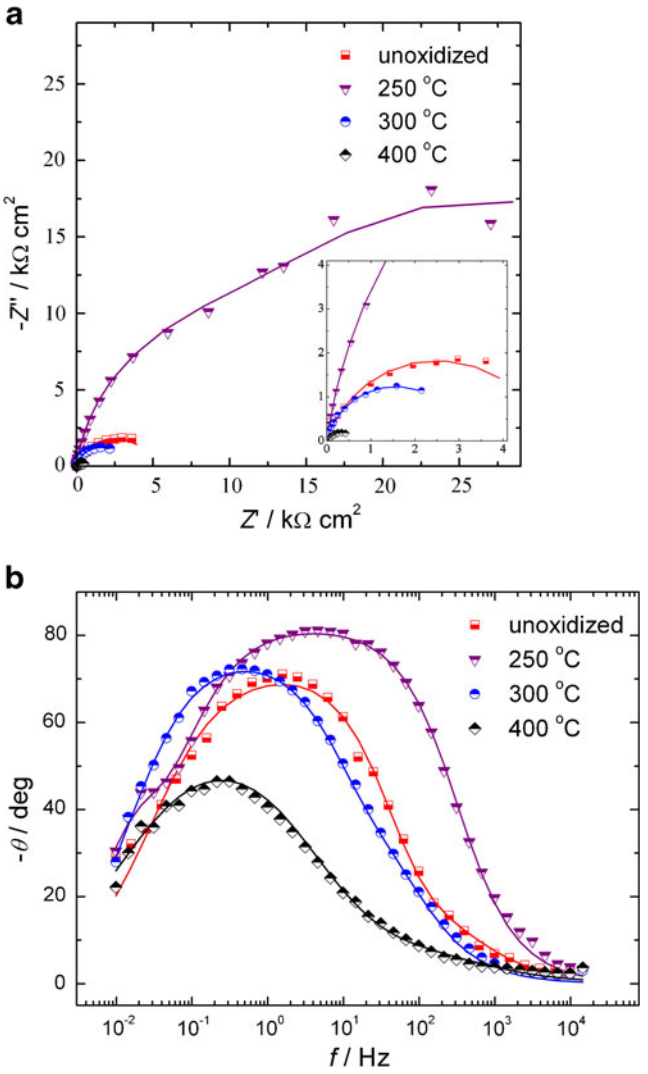

Fig. 7 Impedance plots for specimens without oxidation and with DDT in the test solutions: **a** Nyquist plots; **b** Bode plots. *Symbols*: experimental data; *lines*: fitted values; *insets*: the high frequency parts

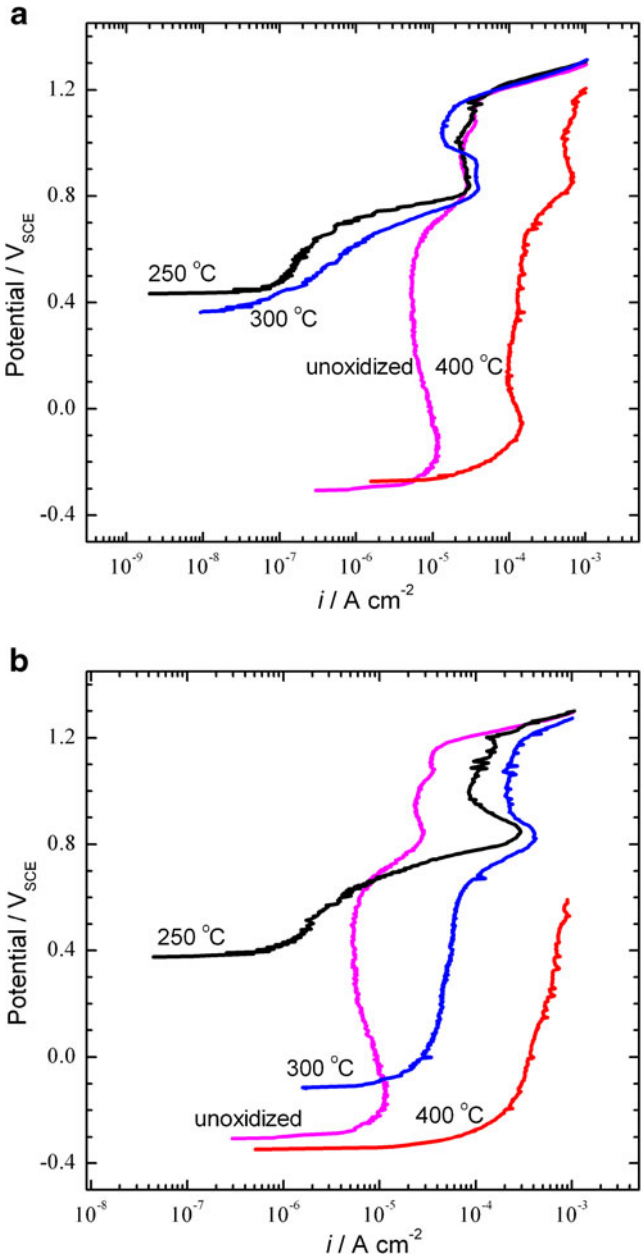

Fig. 8 Anodic polarization curves of specimens without oxidation and with **a** POT and **b** DDT in the test solutions

Discussion

Condensation effect on cyclic oxidation of specimens

In the absence of condensate, the cyclic oxidation process on specimens was simply dominated by the heating temperature. As seen in Fig. 1, 409 SS could form very thin and protective oxide film on its surface after cyclic oxidation at 250 °C or 300 °C, but due to its low chromium content, 409 SS would meet faster oxidation at 400 °C with the occurrence of nodular oxides, which resulted in forming a relatively thick oxide film with low protection to further oxidation.

In comparison with POT (Figs. 1, 2, 3, and 4), the presence of condensates in DDT reduced markedly the oxidation resistance of 409 SS and gave rise to forming defective oxide films under 300 °C and 400 °C conditions. As observed by Sato et al. [8], the condensate ions would evaporate almost completely except small amount of SO_4^{2-} ions over 300 °C. Above analyses also found that sulfur existed as sulfides of Fe and Cr in the oxide films formed with DDT. Furthermore, the inward transport of sulfur might produce sulfides in the metal substrate near the metal/oxide interface during cyclic tests (Fig. 4). It is known that sulfides have more crystal defects than metal oxides [16]. These implied that sulfidation induced by SO_4^{2-} ions was mainly responsible for the accelerated oxidation of 409 SS and formation of defective oxide films on its surface. In addition, because the Pilling-Bedworth ratio (i.e., the volume ratio of oxide to oxidized metal) of $(Fe,Cr)_2O_3$ oxides are

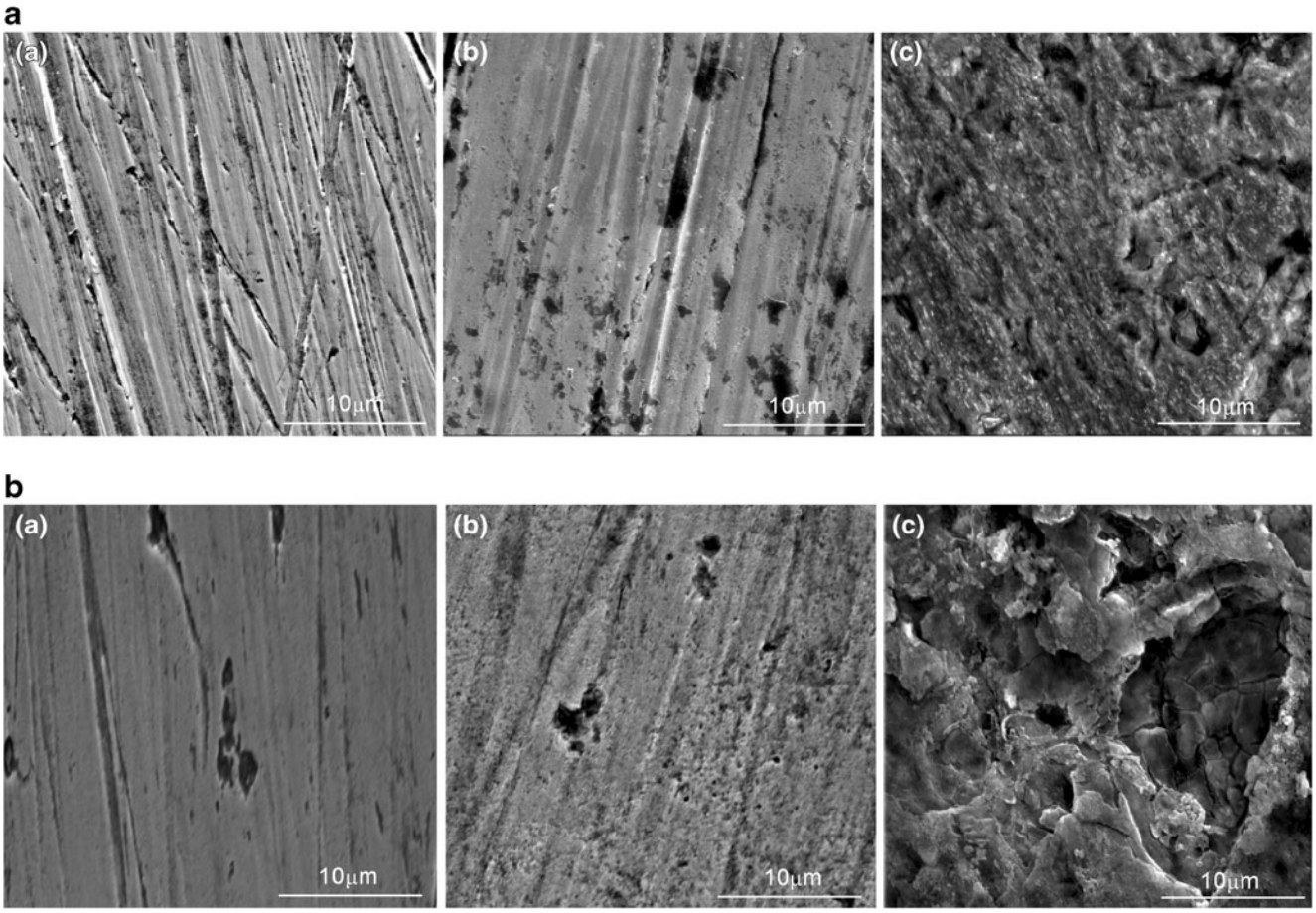

Fig. 9 SEM morphologies of specimens oxidized with **a** POT and **b** DDT after polarization measurements in the test solutions

much higher than 1, the oxidation of 409 SS may induce high compressive stress in the adherent oxide film and corresponding tensile stress in the underlying metal substrate. At the same time, there are thermal stresses in the oxide film resulted from the different thermal expansion coefficients between the metal and film. These stresses may lead to cracking and even spalling of oxide film during the cyclic heating and cooling processes. Apparently, it is reasonable to assume that the growth of oxide film would be accelerated by increasing the oxidation temperature and cyclically dipping condensates, and then created higher mechanic stresses and lattice defects in the film and underlying metal [24, 25].

Electrochemical corrosion of oxidized specimens

It is well known that the corrosion resistance of stainless steel was dependent on the protective oxide film (or passive film) on its surface [26, 27]. Corrosion potential of specimens oxidized with POT at 250 °C and 300 °C or with DDT at 250 °C (Fig. 5) changed slightly in the test solutions and stabilized at values much higher than that of unoxidized 409 SS, which indicated that the oxide films could offer passive protection to 409 SS substrate. However, the oxide films formed with POT at 400 °C or with DDT above 300 °C could not prevent electrolyte penetration because of the defects. The rapid drop in corrosion potential was symbolic of electrolyte penetrating to the oxide/metal interface. As a result, the corrosion potential of oxidized specimens changed to that of unoxidized 409 SS after about 1 h of immersion in the test solutions.

The polarization and impedance measurements confirmed that the corrosion of oxidized specimens changed from passive to active state with increasing oxidation temperature of POT or DDT to 400 °C. To investigate the effect of cyclic oxidation on condensate corrosion, an electrochemical equivalent circuit was proposed in Fig. 10 for the corrosion systems on the basis of the formation of oxide films (or corrosion products films) on the specimen surfaces. R_s represents the electrolyte resistance, R_f and C_f represent the resistance and capacitance of oxide films (or corrosion products films) on the electrode surfaces, R_t and C_{dl} represent the charge transfer resistance and double layer capacitance, respectively. In addition, both C_f and C_{dl} were replaced with constant phase element (CPE) in the fitting procedure due to the non-ideal capacitive response of the

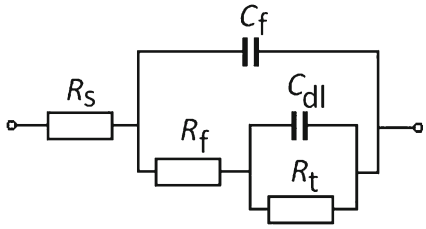

Fig. 10 Equivalent circuit for the corrosion system 409 SS/condensate. R_s, electrolyte resistance; R_f and C_f, resistance and capacitance of oxide films (or corrosion products films); R_t and C_{dl}, charge transfer resistance and double layer capacitance

corrosion system. As shown in Figs. 6 and 7, the simulated data show good coincidence with the experimental data in spite of the approximations made. This indicated that the model provided a reliable description for the corrosion systems. Table 3 gives the fitted values of impedance parameters from measured EIS spectra, where Y_0 is the magnitude of admittance of CPE and α is the exponential term [28]. Pure capacitive behavior is represented by $\alpha=1$. Actually, α is often in the range zero to one.

As for both POT and DDT in Table 3, $Y_{0,f}$ and $Y_{0,dl}$ values increased with changing the temperature from 250 °C to 400 °C whereas R_f and R_t (i.e., the corrosion resistance of specimen) values decreased gradually. These indicated that the oxide films became more defective or porous (Figs. 1 and 2), i.e., worse protection to underlying metals with the increase of oxidation temperature. In addition, Zimina et al. found that, when the pure oxidation of 17Cr1Ti steel was changed from 300 °C to 600 °C, the dissolution of oxide films in H_2SO_4 (pH 1.65) solutions would get easier due to the formation of nonstoichiometric oxides [29, 30]. Therefore, the slow dissolution of oxides might also enlarge the porosity of oxide films.

Compared with unoxidized 409 SS, the oxidized specimens showed much lower R_t values after ten cycles of POT at 400 °C or DDT at 300 °C and 400 °C It could be concluded that the corrosion resistance of 409 SS would be reduced markedly as the temperature of cyclic oxidation increased to 400 °C for POT or 300 °C for DDT. These could be attributed mainly to the active corrosion of the weak Cr-depleted zones through the defects (Figs. 1, 2, and 4). In comparison with POT, DDT led to larger $Y_{0,f}$ and $Y_{0,dl}$ values and lower R_t value at each given temperature in Table 3, especially above 300 °C, as a result of forming thicker but more defective oxide films in the presence of condensate ions (e.g., SO_4^{2-}). Moreover, it is assumed that the sulfides would facilitate the ion diffusion to metal substrate through their crystal defects. The crystal lattice defects and mechanical stresses in the thermal oxide film and underlying metal could also increase the corrosion (or pitting) tendency of stainless steels [24]. Therefore, though specimens oxidized with both POT and DDT at 250 °C were in the passive state, R_t value for POT was about 8.5 times larger than that for DDT due to the big difference in the microstructure of the oxide films.

Mechanistic implication on internal corrosion of cold end components

In practice, the cold end components such as muffler suffer inevitably from the cyclic oxidation and condensation of exhaust gas. It is evident that the condensed electrolyte on their internal surfaces will promote the formation of defective oxide films in heating process and then deteriorates their oxidation resistance. On the other hand, the hot exhaust gas will accelerate condensate corrosion through producing weak Cr-depleted zone, sulfides, and non-protective oxide films by thermal oxidation. Therefore, the cyclic processes of oxidation and condensation act in a synergetic way, leading to the corrosion failure of cold end components such as mufflers.

As for high sulfur-fuel oil, the concentration ratio of SO_4^{2-} to Cl^- is far larger than 1 in the condensed solutions [3, 4, 17, 31]. According to the literature [32–34], Cl^--induced pitting of 409 SS may be inhibited completely as observed in Fig. 8 under all conditions. Obviously, the corrosion perforation of mufflers cannot be attributed to Cl^- ions simply. It is well known that the defects in surface oxide films play a great important role in both active corrosion and passivation of metals [35, 36]. Acidic condensates will be sure to reach metal substrate through the cracks and nodules in the oxide films as well as the crystal defects of sulfides and oxides. As a result, localized corrosion takes place along the defects and evolves into pits, even subsequent

Table 3 Fitted values of impedance parameters for specimens with different cyclic processes

Heating	$R_s/\Omega\ cm^2$	$Y_{0,f}/s^{\alpha}\ \Omega^{-1}\ cm^{-2}$	α_f	$R_f/\Omega\ cm^2$	$Y_{0,dl}/s^{\alpha}\ \Omega^{-1}\ cm^{-2}$	α_{dl}	$R_t/\Omega\ cm^2$
No heating	9.2	6.80×10^{-4}	0.77	11.6	1.27×10^{-4}	0.98	5094
250 °C/POT	8.3	3.64×10^{-5}	0.96	113	1.09×10^{-5}	0.86	3.72×10^{5}
300 °C/POT	6.7	3.74×10^{-5}	0.90	60	1.47×10^{-5}	0.93	2.22×10^{5}
400 °C/POT	6.4	1.68×10^{-3}	0.74	20.7	1.31×10^{-3}	0.82	1694
250 °C/DDT	8.2	8.78×10^{-5}	0.95	26	4.66×10^{-5}	0.84	4.39×10^{4}
300 °C/DDT	5.6	1.38×10^{-3}	0.85	15.2	9.29×10^{-4}	0.86	3091
400 °C/DDT	9.8	3.10×10^{-3}	0.64	6.1	4.77×10^{-3}	0.68	664

perforation. The weak Cr-depleted zone formed at the metal/oxide interface during the cyclic oxidation will facilitate the formation and growth of these pits. So, it is reasonable to believe that the corrosion perforation of mufflers is mostly attributed to the cyclic and synergetic effect of oxidation and condensation processes of hot moisture-bearing exhaust gas. Further work is ongoing to elucidate the mutual effect of thermal oxidation and condensate corrosion (i.e., longer condensate-dipping) in the cyclic process.

Conclusions

The cyclic oxidation resistance of 409 SS depends on the temperature and condensation of hot exhaust gas. In the absence of condensates, cyclic oxidation gives rise to form protective oxide films at 250 °C and 300 °C but nodular oxide film at 400 °C. Depositing condensate ions such as sulfate cyclically on steel surface accelerates the thermal oxidation process, leading to form defective oxide films. Weak depletion of chromium occurs underlying the oxide films, especially under 400 °C oxidation conditions. The oxide films are composed of $(Fe,Cr)_2O_3$ and small amount of Fe_3O_4 and sulfides.

Cyclic oxidation below 400 °C affects the corrosion resistance of 409 SS in the simulated automotive condensate solutions on the basis of high sulfur-fuel oil. Without dipping condensates, the oxidation below 300 °C enhances greatly the passive impedance of 409 SS, but the oxidation at 400 °C almost results in active corrosion at the free corrosion potential. With cyclically dipping condensates, the oxidation at 250 °C may still offer passive protection to 409 SS, but the oxidation higher than 300 °C deteriorates its corrosion resistance, even into active corrosion of weak Cr-depleted zones. Furthermore, 409 SS shows much lower corrosion resistance after the cyclic oxidation with condensate-dipping than that without condensate-dipping at each given oxidation temperature, which results mainly from the difference in defective structure of oxide films induced by the growth stress and sulfidation. Besides chloride ions, acidic condensate corrosion through the defects of oxide films may be another important factor for the perforation of muffler.

Acknowledgements Financial support provided by Natural Science Foundation of China (NSFC, grant no. 51134010) and Shanghai Leading Academic Discipline Project (S30107) is greatly appreciated.

References

1. Atsushi M, Junichiro H, Osamu F (2004) JFE Tech Rep 4:61–66
2. Inoue Y, Kikuchi M (2003) Nippon Steel Tech Rep 88:62–69
3. Douthett J (2006) Automotive Exhaust System Corrosion. In: Cramer SD, Covino BS, Jr (eds) ASM Handbook Vol. 13C, Corrosion: Environments and Industries. ASM International, Materials Park, Ohio, pp 519–530
4. Ujiro T, Kitazawa M, Togashi F (1994) Mater Perform 33:49–53
5. Chang S, Jun JH (1999) J Mater Sci Lett 18:419–421
6. Doche ML, Hihn JY, Mandroyan A, Maurice C, Hervieux O, Roizard X (2006) Corros Sci 48:4080–4093
7. Miyazaki A, Hirasawa J, Satoh S (2000) Kawasaki Steel Tech Rep 43:21–28
8. Sato E, Tanoue T (1995) Nippon Steel Tech Rep 64:13–19
9. Sabata A, Brossia C, Behling M (1998) CORROSION/98, paper no. 549. NACE International, Houston, TX, pp 1–25
10. Lee SU, Ahn JC, Kim DH, Hong SC, Lee KS (2006) Mater Sci Eng A 43:155–159
11. Kim D, Kim H (2008) J Korean Inst Met Mater 46:652–661
12. AK Steel (2007) Aluminized steel type 1 stainless 409 and 439, Product Data Bulletin, pp1-5. (www.aksteel.com)
13. Allegheny Ludlum (1999) Stainless steel AL 409HP, Technical Data Blue Sheet, pp1-10. (www.alleghenyludlum.com)
14. Tsaur CC, Rock JC, Wang CJ, Su YH (2005) Mater Chem Phys 89:445–453
15. Mohanty BP, Shores DA (2004) Corros Sci 46:2893–2907
16. Wang CJ, He TT (2002) Oxide Met 58:415–437
17. Chen C, Shang CJ, Weng JY, Li DY (2010) Adv Mater Res 89–91:102–106
18. Zurek Z, Gilewicz-Wolter J, Hetmanczyk M, Dudala J, Stawiarski A (2005) Oxide Met 64:379–395
19. Hamadou L, Kadri A, Benbrahim N (2010) Corros Sci 52:859–864
20. Ferreira MGS, Hakiki NE, Goodlet G, Faty S, Simoes AMP, Belo MDC (2001) Electrochem Acta 46:3767–3776
21. Mandrino D, Godec M, Torkar M, Jenko M (2008) Surf Interface Anal 40:285–289
22. Ramasubramanian N, Preocanin N, Davidson RD (1985) J Electrochem Soc 132:793–798
23. Ye W, Li Y, Wang FH (2009) Electrochim Acta 54:1339–1349
24. Esih I, Alar V, Juraga I (2005) Corros Eng Sci Technol 40:110–120
25. Dah EN, Tsipas S, Hierro MP, Perez FJ (2007) Corros Sci 49:3850–3865
26. Olsson COA, Landolt D (2003) Electrochim Acta 48:1093–1104
27. Schmuki P (2002) J Solid State Electrochem 6:145–164
28. Hsu CH, Mansfeld F (2001) Corrosion 57:747–748
29. Zimina T, Oshe E, Dubkov V, Zimin P, Zabrodskaya E (1998) J Electrochem Soc 145:2236–2240
30. Zimina T, Tselykh O, Oshe E (2004) Prot Met 40:641–645
31. Chol YS, Shin DH, Kim JG (2007) Corrosion 63:522–528
32. Leckie HP, Uhlig HH (1966) J Electrochem Soc 113:1262–1267
33. Pistorius PC, Burstein GT (1992) Corros Sci 33:1885–1887
34. Pistorius PC, Burstein GT (1994) Corros Sci 36:525–538
35. Macdonald DD, Urquidi-Macdonald M (1986) Electrochim Acta 31:1079–1086
36. Macdonald DD (1992) J Electrochem Soc 139:3434–3448